Earth and Planetary Science Letters 377–378 (2013) 287–298

Contents lists available at SciVerse ScienceDirect

Earth and Planetary Science Letters

www.elsevier.com/locate/epsl

Global Positioning System constraints on the active tectonics of NE Iran and the South Caspian region

Z. Mousavi [a,b,*], A. Walpersdorf [a], R.T. Walker [c], F. Tavakoli [b], E. Pathier [a], H. Nankali [b], F. Nilfouroushan [d], Y. Djamour [b]

[a] ISTerre, Université Joseph Fourier, CNRS UMR 5275, Grenoble, France
[b] National Cartographic Center, Geodetic Department, Tehran, Iran
[c] Department of Earth Sciences, University of Oxford, South Parks Road, Oxford, OX1 3AN, UK
[d] Department of Earth Sciences, Uppsala University, Villavägen 16, 75236 Uppsala, Sweden

ARTICLE INFO

Article history:
Received 28 September 2012
Received in revised form 11 June 2013
Accepted 5 July 2013
Available online 19 August 2013
Editor: Y. Ricard

Keywords:
Iran
GPS
active deformation
Kopeh Dagh
Alborz
Binalud

ABSTRACT

We present a velocity field compiled from a network of 27 permanent and 20 campaign GPS stations across NE Iran. This new GPS velocity field helps to investigate how Arabia–Eurasia collision deformation is accommodated at the northern boundary of the deforming zone. The present-day northward motion decreases eastward from 11 mm/yr at Tehran (∼52°E) to 1.5 mm/yr at Mashhad (∼60°E). N–S shortening across the Kopeh Dagh, Binalud and Koh-e-Sorkh ranges sums to 4.5 ± 0.5 mm/yr at longitude 59°E. The available GPS velocities allow us to describe the rigid-body rotation of the South Caspian about an Euler pole that is located further away than previously thought. We suggest that two new stations (MAVT and MAR2), which are sited far from the block boundaries, are most likely to indicate the full motion of the South Caspian basin. These stations suggest that NW motion is accommodated by right-lateral slip on the Ashkabad fault (at a rate of up to 7 mm/yr) and by up to 4–6 mm/yr of summed left-lateral slip across the Shahroud left-lateral strike-slip system. Our new GPS results are important for assessing seismic hazard in NE Iran, which contains numerous large population centers and possesses an abundant historical earthquake record. Our results suggest that the fault zones along the eastern Alborz and western Kopeh Dagh may accommodate slip at much faster rates than previously thought. Fully assessing the role of these faults, and the hazard that they represent, requires independent verification of their slip-rates through additional GPS measurements and geological fieldwork.

1. Introduction

Active faulting in Iran results from the continental collision between Arabia and Eurasia. The distribution of earthquake epicenters (Fig. 1) shows that most of the deformation is accommodated within the political borders of the country. GPS measurements also illustrate a similar pattern, with velocities of stations relative to Eurasia decreasing to zero at both the northern and eastern borders of Iran (Vernant et al., 2004). South of our study region (Fig. 1), the N–S right-lateral shearing between western Afghanistan (which is part of stable Eurasia) and central Iran is accommodated on N–S right-lateral faults within eastern Iran (e.g. Walker and Jackson, 2004; Meyer and Le Dortz, 2007). Further north, however, the pattern of faulting is more complex and involves thrusts and left-lateral faults west of ∼58°E and right-lateral strike-slip faults east of ∼58°E. The pattern of faulting must also accommodate motion of the South Caspian Basin relative to its surroundings, though the form that this motion takes is debated (e.g. Jackson et al., 2002; Copley and Jackson, 2006; Djamour et al., 2010).

In recent years, constraints from GPS, earthquake investigations, and geological estimates of fault slip-rate have allowed considerable advances in understanding the rates and kinematics of faulting across many parts of Iran (e.g. Tatar et al., 2002; Jackson et al., 2002; Allen et al., 2003; Nilfouroushan et al., 2003; Talebian and Jackson, 2004; Vernant et al., 2004; Masson et al., 2005; Hessami et al., 2006; Walpersdorf et al., 2006; Tavakoli et al., 2008; Djamour et al., 2010, 2011). Until now, however, there have been few constraints on the present-day distribution of deformation across the eastern and northeastern parts of the country. The rates of faulting are largely unknown, as is the relationship between the active faults and the overall tectonic motions. Furthermore, North Eastern Iran is one of the most densely populated parts of the country with almost 6.5 million inhabitants. The region has an abundant historical record of destructive earthquakes, including the Qumis 856 A.D. earthquake that killed 200,000 people (e.g.

* Corresponding author at: ISTerre, Université Joseph Fourier, CNRS UMR 5275, Grenoble, France.
E-mail address: zahra.mousavi@ujf-grenoble.fr (Z. Mousavi).

0012-821X/$ – see front matter
http://dx.doi.org/10.1016/j.epsl.2013.07.007

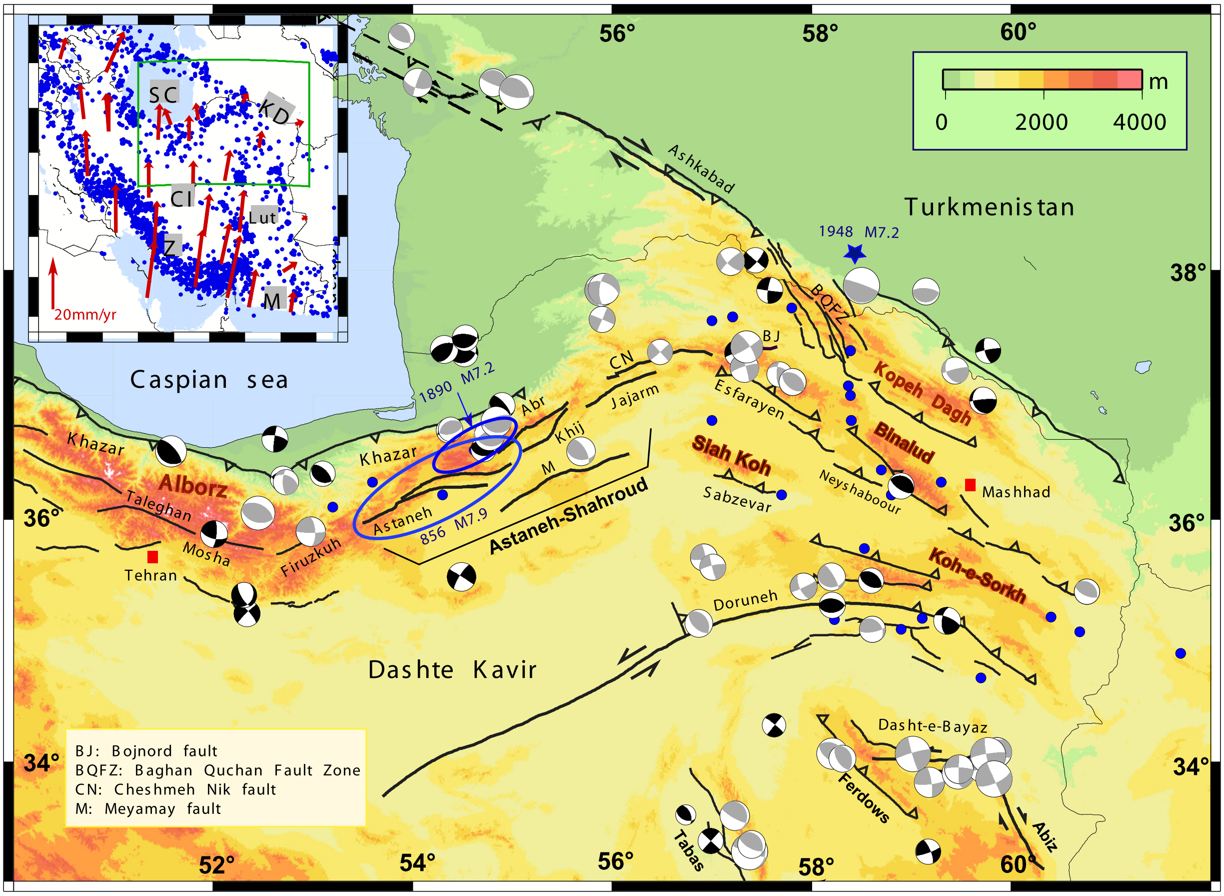

Fig. 1. Inset: Outline map of Iran with GPS velocities relative to Eurasia (Vernant et al., 2004). Epicenters of earthquakes Mw ⩾ 5 in the period 1976–2012 are shown as dots (from the Harvard catalogue http://www.globalcmt.org/CMTsearch.html). The rectangle indicates the location of the map in the main figure. The abbreviations are CI: Central Iran, KD: Kopeh Dagh, Lut: Lut block, M: Makran subduction zone, SC: South Caspian basin, Z: Zagros. Main figure includes topographic map, known active faults and earthquake catalogue epicenters (Mw ⩾ 5). The grey focal mechanisms are first-motion and waveform-modeled solutions from McKenzie (1972), Baker et al. (1993), Berberian and Yeats (1999), Jackson et al. (2002), Walker and Jackson (2004) and Engdahl et al. (2006). The black focal mechanisms are moment tensor solutions from the Harvard catalogue http://www.globalcmt.org/CMTsearch.html during the period 1976–2012. Historical earthquakes (small dots) come from Ambraseys and Melville (1982). The blue ellipsoids and star are the location of 856 AD (M7.9), 1890 (M7.2) and Ashkabad 1948 (M7.2) (Ambraseys and Melville, 1982; Hollingsworth et al., 2010b). (For interpretation of the references to color in this figure legend, the reader is referred to the web version of this article.)

Ambraseys and Melville, 1982; Hollingsworth et al., 2010b). The widespread occurrence of significant earthquakes across NE Iran is less apparent, however, in instrumentally-recorded seismicity (e.g. Fig. 1); there is hence a large societal motivation in characterizing the slip directions and rates of movement across the active fault zones.

Here, we present a velocity field, composed of 47 GPS stations (20 campaign-mode and 27 permanent stations) and recorded over 11 years, which covers almost the entire NE of Iran. We use these velocities to refine estimates of the motion of the South Caspian Block relative to its surroundings, to estimate the present-day slip-rate across the major fault systems of the region (making comparisons to geomorphological and geological estimates where available), and to examine the likely kinematics of faulting in NE Iran. We suggest that some of the fault zones in NE Iran may have much faster slip-rates than is sometimes thought.

2. GPS data and processing

We incorporate both campaign and permanent GPS stations in our network. Campaign measurements were performed from 1999 to 2008 within a framework of French–Iranian cooperation with the support of the National Cartography Center in Tehran. Of the campaign stations, 10 (SHAM, JANA, GRME, GARD, DARG, BAKH, MAR2, KHAF, DOGH and BAJE) were installed and measured in 2004 and three other stations (BIAR, ESFN and ZVNG) were installed and measured in 2005. All these stations were re-measured in 2006 (Tavakoli, 2007). Measurements were made with Ashtech Z12 or Trimble 4000SSI receivers with choke-ring antennas at least for 48 h. We also included five campaign stations (YAZT, SHIR, KORD, SEMN and KASH) in our study that were installed in 1999 by Nilforoushan et al. (2003). The campaign measurements are processed together with measurements from 27 stations of the Iranian Permanent GPS Network (IPGN). The permanent sites were installed in 2005–2006 and are all equipped with Ashtech CGRS receivers and choke ring antennas.

All campaign and IPGN sites were processed using the GAMIT/GLOBK software, version 10.4 (Herring et al., 2006) along with 28 GPS stations of the International GNSS Service (IGS) network in order to produce a stable reference frame. Daily positioning solutions were calculated along with the tropospheric zenith delays at each station every two hours from GPS phase observations, adjusting IGS final orbits and using coherent Earth orientation parameters (EOP). The variation of antenna phase centers is modeled using the absolute antenna phase center model IGS_05. The tropospheric mapping function VMF1 (Boehm et al., 2006) for tropospheric delay and FES2004 ocean tide model for ocean loading (Lyard et al., 2006) were used in the daily processing.

The daily solutions of permanent and campaign networks are combined with global daily solutions using the Kalman filter

Table 1
Site coordinates and horizontal velocities (mm/yr) with respect to Eurasia and observation span for North East Iran GPS stations. The stations with star are permanent stations of IPGN network. 10 stations (GRGN, KORD, MABD, ROBA, SEMN, SHIR, SMNN and TEHN) are published in Djamour et al. (2010) using the reduced data set.

Site	Long	Lat	Ve	Vn	sig Ve	sig Vn	Correlation	Time span
BAJE	58.21463	34.55838	−1.12	6.4	0.4	0.4	0	2004, 2006
BAKH	60.36017	35.00179	0.7	0.19	0.47	0.47	−0.001	2004, 2006, 2007
BIAJ	55.80518	36.08609	1.11	8.66	0.28	0.22	−0.001	2006–2011
BIAR	55.90606	35.98844	0.24	8.94	0.56	0.57	−0.013	2005, 2006, 2007
BOJD	57.27158	37.48033	−2.24	4.96	0.21	0.2	−0.002	2005–2011
DARG	57.58928	35.91483	−1.1	5.64	0.46	0.46	−0.005	2004, 2006, 2008
DOGH	58.86932	35.1084	−0.18	4.73	0.46	0.47	0.002	2004, 2006, 2007
ESFA	57.42698	37.1588	−0.19	4.46	0.54	0.55	−0.002	2005, 2006, 2007
ESFN	57.49458	37.04951	1.06	5.24	0.4	0.25	−0.002	2006–2011
FARM	59.84298	35.69612	0.27	1.99	0.21	0.24	−0.002	2005–2011
FERD	58.18307	34.03065	−1.29	7.96	0.24	0.3	0	2006–2011
GARD	59.19725	35.49547	−0.85	2.53	0.45	0.45	−0.002	2004, 2006
GOLM	59.24776	36.55822	1.37	3.45	0.3	0.2	−0.002	2005–2011
GONA	58.68354	34.37307	−0.58	6.28	0.2	0.16	−0.003	2005–2011
GRGN	54.35327	36.87576	−3.06	6.36	0.23	0.41	0	2006–2011
GRME	56.26434	37.04163	−1.56	7.83	0.46	0.46	−0.001	2004, 2006
JANA	59.07557	37.41278	−1.31	−0.84	0.46	0.46	−0.001	2004, 2006
KADN	58.87825	35.59173	−2.41	2.16	0.46	0.26	0	2005–2011
KALT	59.64043	36.3913	0.6	0.76	0.4	0.25	−0.001	2005–2011
KASH	58.46361	35.29268	−0.91	4.79	0.38	0.38	0	1999, 2001, 2005
KHAF	60.1103	34.58881	−0.36	0.3	0.41	0.41	0.002	2004, 2006, 2007
KHUR	55.08126	33.76931	0.1	11.29	0.23	0.18	−0.002	2006–2011
KORD	54.19946	36.86046	−2.89	5.61	0.31	0.31	−0.002	1999, 2001, 2004, 2005, 2006
KSHM	58.473	35.27057	1.03	5.24	0.2	0.18	−0.002	2005–2011
MABD	52.28515	36.5884	−4.62	6.23	0.27	0.22	−0.001	2005–2011
MAR2	55.95556	37.8445	−5.39	5.5	0.49	0.51	0.001	2004, 2006, 2007
MAVT	55.94386	37.80098	−4.8	5.78	0.34	0.16	−0.001	2006–2011
MSHN	59.47982	36.33472	−0.94	1.45	0.21	0.14	0.001	2002–2011
NFRD	59.40127	36.45012	2.22	4.69	0.31	0.19	−0.002	2007–2011
NISH	58.82026	36.20704	−0.54	4.7	0.25	0.27	−0.001	2005–2011
QAE2	59.18771	33.66336	−0.93	4.53	0.41	0.41	0.001	2004, 2006
QAEN	59.17603	33.73995	−0.4	5.16	0.24	0.23	−0.002	2005–2011
QUCH	58.53728	37.07071	0.63	1.89	0.29	0.19	−0.002	2005–2011
ROBA	56.06975	33.36854	−0.12	9.36	0.29	0.29	−0.001	1999, 2001, 2004, 2005, 2006, 2007
SABZ	57.65283	36.18494	1.47	7.17	0.25	0.26	−0.002	2005–2011
SAFI	57.92129	36.69815	0.41	4.69	0.44	0.22	−0.001	2006–2011
SARK	61.14859	36.53682	−0.73	0.82	0.22	0.21	−0.002	2005–2011
SEMN	53.56365	35.66234	−0.04	8.75	0.38	0.38	0.001	1999, 2001, 2005
SHAM	58.43098	37.56989	−1.79	2.3	0.46	0.46	−0.003	2004, 2006
SHIR	57.30783	37.81392	−4.15	3.15	0.31	0.31	−0.001	1999, 2001, 2004, 2005, 2006, 2008
SHKH	60.29616	33.65433	0.22	0.89	0.46	0.46	0	2005, 2006, 2007
SMNN	53.42068	35.58822	0.41	9.87	0.26	0.15	−0.001	2005–2011
TABS	56.95069	33.60341	−0.63	9.55	0.32	0.2	−0.001	2006–2011
TEHN	51.33409	35.69728	−1.52	11.19	0.23	0.16	−0.001	2000–2011
THED	59.2187	35.34695	0.27	3.72	0.2	0.21	−0.002	2005–2011
TJAM	60.56424	35.29435	0.62	2.97	0.33	0.31	−0.003	2006–2011
TORQ	59.6275	36.22409	0.92	0.36	0.27	0.27	−0.001	2005–2011
TOTI	58.53149	33.01918	−0.69	7.59	0.49	0.49	−0.004	2006, 2007
TOUS	59.48908	36.44502	0.17	−4.38	0.57	0.25	−0.001	2004–2011
YAZT	61.03374	36.60135	−1.33	0.03	0.31	0.31	0	1999, 2001, 2004, 2005
ZVNG	58.51467	36.43843	1.09	3.4	0.54	0.55	−0.005	2005, 2006, 2007, 2008

GLOBK to calculate a consistent set of coordinates and velocities. Before estimating the velocity field, we clean all time series from outlier and offsets. Then a unique noise model for each permanent station is calculated to account for correlated errors in the time series analysis. The algorithm used to model the data noise spectrum assumes that each time series can be adequately modeled using a first-order Gauss Markov (FOGM) process noise (Gelb, 1974; Reilinger et al., 2006; Djamour et al., 2010).

The FOGM model is estimated from individual stations' time series by averaging the residuals over increasingly longer intervals that range from a minimum of 7 days to a maximum of 1/10th of the total time series span. Then this model is used to predict the site velocity uncertainty based on the time span of the time series (Reilinger et al., 2006; Djamour et al., 2010). GLOBK could calculate the Random Walk (RW) noise model that would predict the same velocity uncertainty as the FOGM model at the time series time span interval. These RW process noise values are then used in the forward run of the GLOBK Kalman filter (using the same data as was used in the time series) to estimate site velocities and "realistic" uncertainties. Since this method of estimating site-dependent process noise is only applicable to continuous time series (as we need to be able to average over a range of time series sampling intervals), the RW process noise applied to campaign GPS sites in the North East Iran region was obtained by taking the median of the RW values for permanent sites in the region. This noise for North East Iran ranges from 0.32 to 1.3 mm/$\sqrt{}$(yr) with a median of 0.8 mm/$\sqrt{}$(yr) for horizontal and 1.1 to 4.3 mm/$\sqrt{}$(yr) with a median of 2.7 mm/$\sqrt{}$(yr) for vertical components. We used these median values for RW noise of campaign stations to obtain realistic velocity uncertainties. The Eurasia-fixed coordinate and velocity file of ITRF2008 (Altamimi et al., 2011) is used to establish the Eurasian reference frame and to calculate the velocity field of the Kopeh Dagh network with respect to stable Eurasia as presented in Table 1 and Fig. 2.

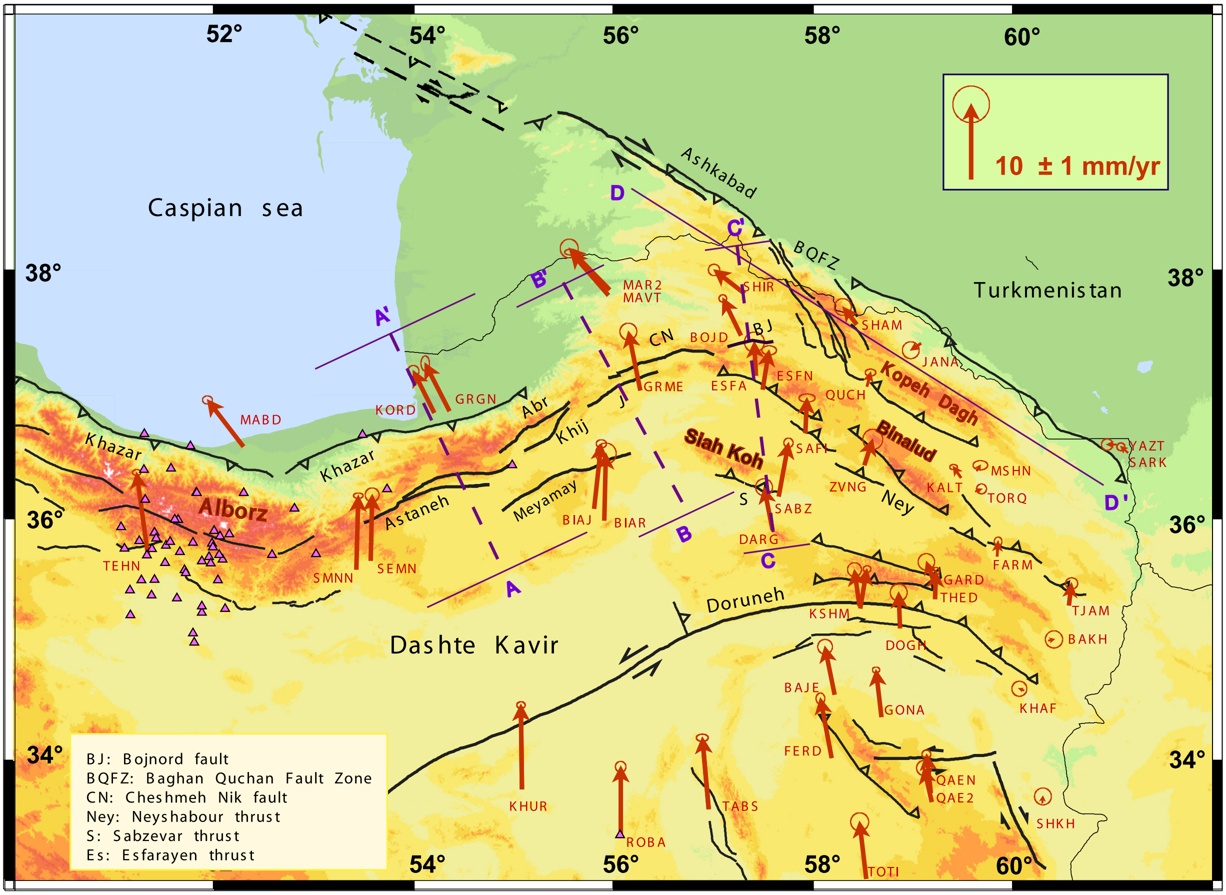

Fig. 2. Velocity field for the North East of Iran is shown with respect to Eurasia. The velocity field includes both campaign and permanent GPS stations. The scale vector corresponds to 10 mm/yr. The triangle symbols represent the GPS stations from Djamour et al. (2010), which are included in our block modeling analysis. The boxes AA', BB', CC' and lines DD' indicate the locations of cross sections presented in Fig. 5.

3. Geodetic velocity field in NE Iran

The GPS stations in the southern part of our study area (at latitudes below ∼34°, Fig. 2) show northward-directed velocities increasing linearly from zero at the eastern margin of Iran (e.g. stations SHKH, KHAF) to ∼11 mm/yr (KHUR), consistent with distributed N–S right-lateral shear accommodated on N–S right-lateral faults across the eastern part of Iran south of latitude 34°N (Walker and Jackson, 2004; Vernant et al., 2004; Meyer and Le Dortz, 2007). The same general pattern is seen in northerly parts (about 36°N) of the velocity field, with effectively zero velocity relative to Eurasia at Sarakhs (SARK) increasing to 11 mm/yr at Tehran (TEHR).

Stations in the NW of our network show a northwestward motion with respect to Eurasia. These northwestern stations are likely to represent motion of the South Caspian block (e.g. Djamour et al., 2010). The South Caspian Basin is an aseismic block that is surrounded by belts of intense earthquake activity (e.g. Jackson et al., 2002; Hollingsworth et al., 2008). The basement of the South Caspian Basin may be thick oceanic crust (Mangino and Priestley, 1998) that is beginning to subduct beneath the continental crust of the northern Caspian Basin. The South Caspian Block appears to be moving relative to its surroundings, with this motion accommodated by deformation at its boundaries, along which the Ashkabad and Astaneh–Shahroud fault systems are situated (Fig. 1). However, to calculate the rates of slip at the boundaries of the South Caspian we must constrain its motion relative to Eurasia and Iran. This motion has been described both as a rigid-body rotation about an Euler pole sited east of the Caspian Sea (Djamour et al., 2010), and as a rotation about a pole far away from it (e.g. Jackson et al., 2002). Finding the correct description has large implications for the slip-rates calculated from the GPS measurements.

Jackson et al. (2002) use a plate-closure model to predict a rigid-body motion of the South Caspian Block relative to Eurasia at a rate of 7–10 mm/yr and azimuth 300°. Copley and Jackson (2006) revised these estimates to $\sim 11 \pm 2$ mm/yr at an azimuth of 330–340°. Copley and Jackson's (2006) estimate of the South Caspian motion yields 4.5–5.5 mm/yr of shortening and left-lateral strike-slip across the Alborz and 7–11 mm/yr of right-lateral strike-slip across the Ashkabad fault (assuming that all fault motion is localized onto this one structure). An alternative interpretation of the kinematics of the South Caspian was provided by Djamour et al. (2010), who constrained its motion with GPS stations near the southern shore of the Caspian sea (TKBN, KORD, GRGN, MAHM, NKAD) and a sixth (SHIR) sited at the eastern end of the eastern Caspian lowlands. From these six stations they estimated the motion of the block as a clockwise rotation relative to Eurasia with an Euler pole located much closer to the basin at 59.1°E and 40.4°N (Fig. 3). The presence of this rigid-body rotation has a significant effect on the slip-rates calculated for the fault zones that surround the block. For instance, using the block motions calculated by Djamour et al. (2010), a right-lateral slip-rate of only ∼3 mm/yr is calculated for the Ashkabad fault; a figure that is less than half that calculated by Jackson et al. (2002) and Copley and Jackson (2006), and which has large implications for the assessment of hazard.

To refine estimates of the motion of the South Caspian we have added data from 2 new permanent GPS stations (BOJD and MAVT), one new campaign station (MAR2), and have updated the velocity for station SHIR, which is now shown to be faster and directed

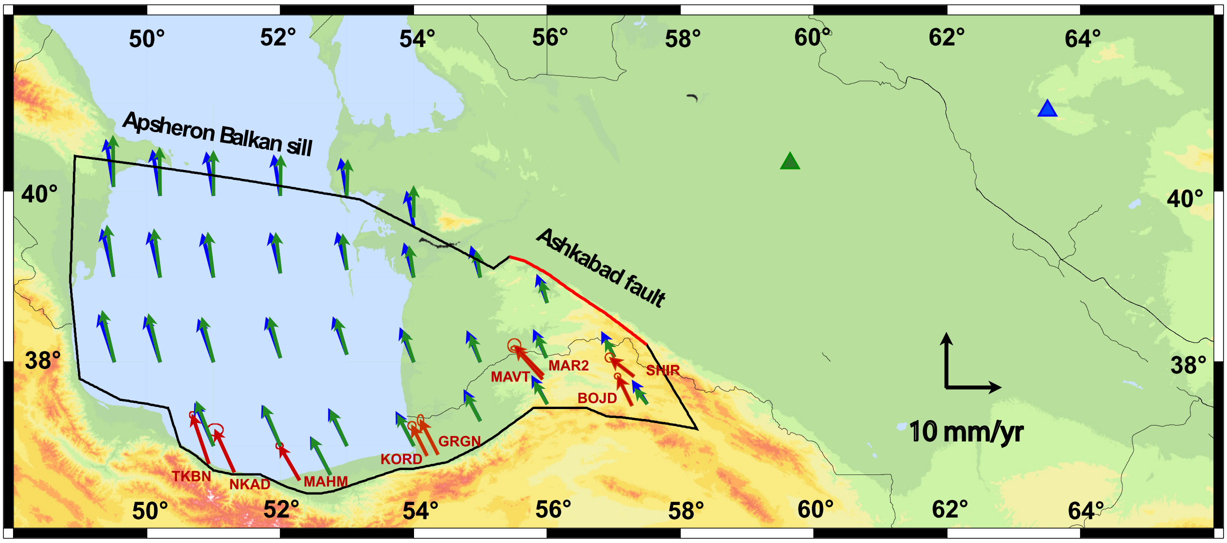

Fig. 3. Map showing the location of South Caspian Euler pole with respect to Eurasia and the predicted block motion without taking into account the interseismic elastic strain along the block boundaries. The green vectors and Euler pole (represented by a triangle) show the predicted block motion of the SCB using 6 GPS stations (GRGN, KORD, MAHM, NAKD, SHIR and TKBN) by Djamour et al. (2010). The blue vectors and triangle indicate the predicted block motion of the SCB using 9 GPS stations (BOJD, GRGN, KORD, MAHM, MAR2, MAVT, NAKD, SHIR and TKBN). Note that there is still a large difference between the predicted and observed motion of stations MAVT and MAR2, which are the only stations to lie well within the interior of the block. (For interpretation of the references to color in this figure legend, the reader is referred to the web version of this article.)

more to the west than previously estimated. Adding these new and updated stations yields an Euler pole for rotation of the South Caspian that has moved 400 km to the NW from the pole calculated by Djamour et al. (2010) to lie at 59.1°E and 40.4°N (Fig. 3). However, even with the revised Euler pole, there are still large residuals between the motions predicted from the block model and the observations from the MAVT and MAR2 stations (Fig. 3).

Much of the difficulty in estimating the motion of the South Caspian block is that most of its interior is covered by water, such that most measurements are made at its boundaries, in locations that may be contaminated by elastic strain accumulation. For instance, the SHIR and BOJD stations are sited within the central Kopeh Dagh, in a region of high topography, and in which large earthquakes have occurred in recent decades (Figs. 1 and 2). It is hence doubtful that they are representative of the full motion of the South Caspian. Similar arguments can be made for the stations along the southern boundary of the South Caspian, which are all situated close to the deforming Alborz range and therefore may be affected by elastic deformation at the block boundary. The two new stations MAVT and MAR2 are thus extremely important, given the uncertain degree to which any of the other GPS stations are representative of the motion of the interior of the South Caspian. Both are situated within a region of low-lying topography far from the major fault systems, and are therefore the most likely to be representative of the block motion. These stations, MAVT (permanent) and MAR2 (campaign) are located within 3 km of each other and are sited on pillar constructions. The time series of MAVT station does not show any outliers or jumps in five years of measurement. Their individual velocities (~7 mm/yr at 317°N relative to Eurasia) are coherent and are comparable to the 7–10 mm/yr and azimuth 300°N estimation of the South Caspian motion of Jackson et al. (2002) but clearly lower than the ~11 ± 2 mm/yr at an azimuth of 330–340° proposed by Copley and Jackson (2006).

Taking only the two coherent MAR2 and MAVT velocities to represent the motion of the South Caspian with respect to its surroundings yields upper limits on the slip-rates across the Shahroud and Ashkabad faults. By using all available GPS stations to evaluate a rigid South Caspian block motion we obtain a clockwise rotation about an Euler pole at 63.58°E and 41.05°N, yielding lower fault slip-rates at the block boundaries. In the following discussion, we quantify the lower and the upper limits of relative motion across block boundaries by presenting rates computed both from a rigid block model constrained by all available GPS stations and from local profiles of along-fault and across-fault changes in velocity that do not take into account any block rotations.

Changes in the magnitude and orientation of velocities within the GPS network near active faults can be fitted by an arctangent function that is characteristic for elastic strain accumulation (Okada, 1985). GPS station velocities on profiles across the Ashkabad and the Shahrud fault systems are plotted in Figs. 2 and 5. These profiles allow us to provide estimates of the cumulative slip-rate across several of the main faults but, because the GPS measurements are still rather sparse, they do not allow us to assign slip-rates to individual fault strands within these zones. Our GPS velocities are also used to constrain a simple, two-dimensional (2-D) elastic half-space model of rigid block kinematics (using the Defnode code: Meade et al., 2002; McCaffrey, 2002; Meade and Hager, 2005; Reilinger et al., 2006; Djamour et al., 2010). We combine our solution with the velocity field of Djamour et al. (2010) for the Alborz (station locations shown as pink triangles, Fig. 2) to be able to constrain the South Caspian block and the Alborz block. SHIR has a different value in our work as it now has one more measurement epoch in comparison with Masson et al. (2007) and Djamour et al. (2010). No significant earthquake has occurred during the time interval of the measurements in the Alborz (Djamour et al., 2010) and Kopeh Dagh that could affect the GPS velocity field.

For the rigid block model, we define five blocks: The South Caspian Basin (SCB), the Alborz (ALB), the South Doruneh Block (SDB), the Central Iran Block (CIB) and the Eurasian Block (EUB) (Fig. 4). Their boundaries are related to mapped faults, seismicity, and historic earthquakes. SCB is defined using 9 stations (BOJD, GRGN, KORD, MAHM, MAR2, MAVT, NKAD, SHIR and TKBN). The block boundaries coinciding with active faults are shown in dark gray lines while other block limitation that are necessary to close the block boundaries are presented in dotted lines in Fig. 4. We used the Defnode code by McCaffrey

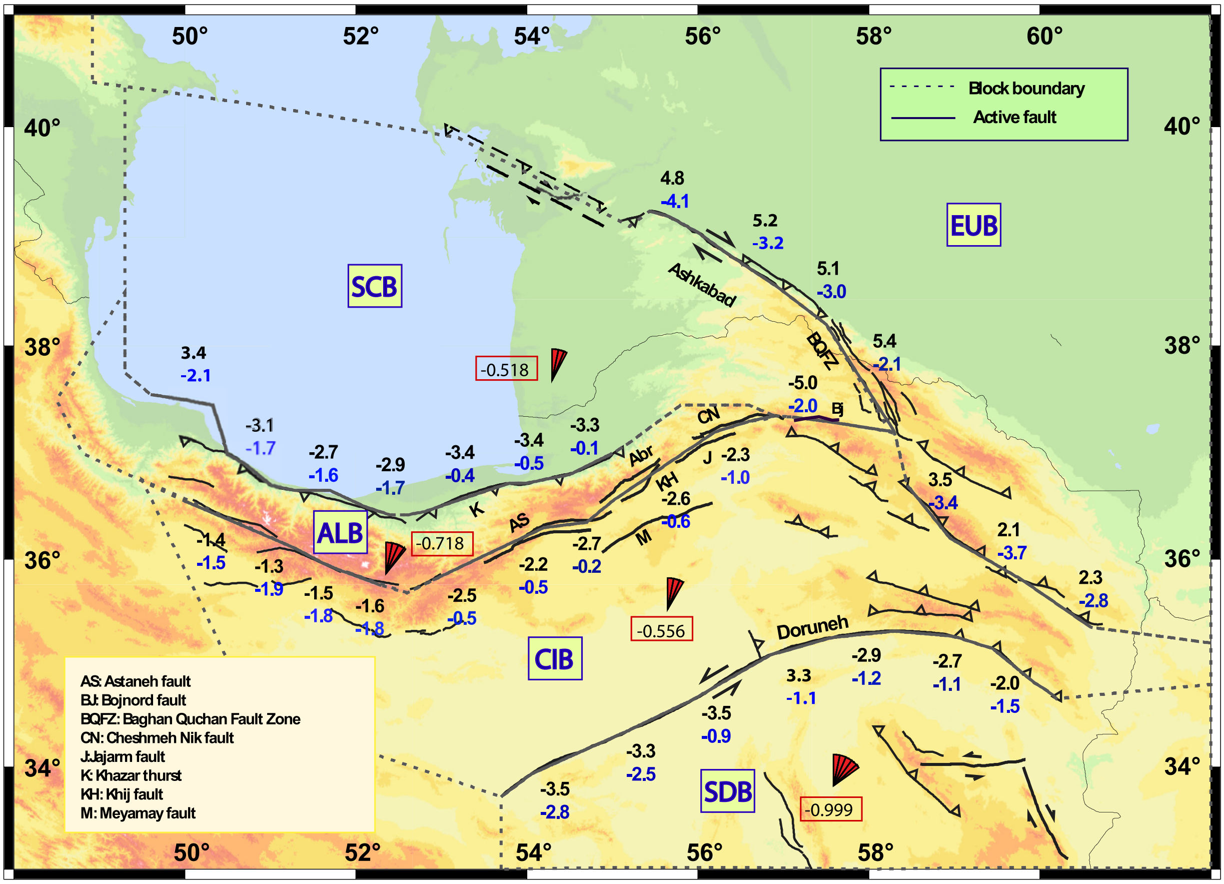

Fig. 4. Map showing slip-rate variability (mm/yr) along the active faults from rigid block modeling. The upper values show the strike-slip component (positive indicates right-lateral slip). The lower values indicate the fault-perpendicular slip-rates (negative values indicate shortening). Dark gray lines represent active faults and dotted lines show block boundaries. The blocks are ALB: Alborz, CIB: Central Iran, EUB: Eurasian, SCB: South Caspian and SDB: South Doruneh blocks. Numbers inside the red rectangles are GPS block rotation rates in °/Ma, in the center of each block, calculated from block modeling with locked faults. Counterclockwise rotation sense is positive. (For interpretation of the references to color in this figure legend, the reader is referred to the web version of this article.)

(2002) to solve for relative block motions by adjusting an Euler pole to the GPS motions within a same block in a least-square sense. We assume that all active faults along the block boundaries are locked to a depth of 15 km, so, realistically, some elastic deformation is taken into account along the block boundaries. The model allows no permanent deformation of the blocks or slip on unconnected faults; this implies that all the faults used must be on a block boundary (Djamour et al., 2010). The WRMS values for estimation of Euler vectors relative to Eurasia for Alborz, South Caspian Basin, Central Iran and South Doruneh blocks are 0.91, 1.07, 1.03, 1.09 mm yr^{-1}, respectively, with no significant systematic residuals. The fault slip-rates estimated from a block model using the Defnode code vary usually by approximately $+/-1$ mm/yr according to a statistical study (Karakhanyan et al., 2013). Thus we consider 1 mm/yr as uncertainty of the fault slip-rates computed by rigid block modeling.

In the following, we examine the constraints that our GPS measurements introduce for the rates of fault slip in individual parts of NE Iran. We present both the slip-rates obtained from the kinematic block modeling, as described above, and from profiles of along-strike and across-strike velocity change across the main fault zones. The profiles assume that no significant rigid-body rotation occurs in the South Caspian. In Section 4, we compare the GPS-derived rates with existing late Quaternary slip-rate measurements. All GPS and late Quaternary rates are listed in Table 2.

3.1. Eastern Alborz and the Astaneh–Shahroud strike-slip fault system

Earthquake slip vectors and large-scale geomorphology imply that deformation across the eastern Alborz is spatially separated (partitioned) into components of shortening on the Khazar thrust at the northern margin of the range and left-lateral strike-slip across the Shahroud fault along the southern slopes of the mountains (Jackson et al., 2002; Tatar et al., 2007; Hollingsworth et al. 2008, 2010a). The Shahroud fault system is itself composed of a series of NE–SW trending segments (Hollingsworth et al., 2008; Javidfakhr et al., 2011a). Along much of its length, the Shahroud fault system is composed of overlapping parallel strands that all display geomorphic indications of recent faulting (Fig. 1, e.g. Hollingsworth et al. 2008, 2010a; Javidfakhr et al. 2011a, 2011b). Several of these segments are likely to be associated with historical earthquakes. For instance, the Astaneh segment may have been responsible for the devastating 856 A.D. Qumis earthquake that killed 200,000 people and the 1890 Shahroud earthquake, with a magnitude of ∼7, is likely to have occurred on the Abr fault segment (Hollingsworth et al., 2010b; Fig. 1).

To evaluate the strike-slip and shortening components across the eastern Alborz, and to examine whether fault slip-rates may vary along the strike of the range, we projected fault-parallel and fault-normal components of GPS velocities onto profiles drawn perpendicular to the faults (AA', BB' and CC', Fig. 2). Profile AA' (Fig. 5) indicates 4.5 ± 0.5 mm/yr of left-lateral slip and 1.8 ± 1.0 mm/yr of shortening across the Alborz at the longitude of the Shahroud fault zone. The block modeling approach provides lower estimates

Table 2
Long term and current fault slip-rates of the major active faults in North East Iran, 1. Trifonov (1978); 2. Lyberis and Manby (1999); 3. Fattahi et al. (2006b); 4. Hollingsworth et al. (2006); 5. Fattahi and Walker (2007); 6. Masson et al. (2007); 7. Hollingsworth et al. (2008); 8. Shabanian et al. (2009a); 9. Siame et al. (2009); 10. Djamour et al. (2010); 11. Hollingsworth et al. (2010a); 12. Hollingsworth et al. (2010b); 13. Javidfakhr et al. (2011a); 14. Rizza et al. (2011); 15. Shabanian et al. (2012); 16. Walters et al. (2013). Numbers with star are the geologic slip-rate without age constraint. The abbreviations are SH: shortening, LL: left lateral and RL: right-lateral.

Fault name	Geodetic (mm/yr)	Block modeling (mm/yr)	Geologic (mm/yr)	Geologic time (kyr)
Shahroud Abr & Khij at 55°E Cheshmeh & Jajarm at 56°E	4.1–6.5 LL	2.4 ± 1 LL, 0.8 ± 1 SH	3–4 (Abr) + 1–3 (Khij) LL (13)	115 ± 14 (13)
Astaneh Eastern Khazar thrust	4.3 ± 0.5 LL, 1.8 ± 0.8 SH	2.5 ± 1 LL, 2 ± 1 LL (10) 3.3 ± 1 LL, 2–3 SH (10), 5 ± 2 LL (10)	1–7–2.5* LL (12), ∼2 LL (14) –	32–55 (14) –
Bojnord	4.1 ± 1.5 LL	5.0 ± 1 LL, 2.0 ± 1 SH	–	–
Ashkabad	6.7 ± 0.5 RL, 1.5–3.5 SH, ∼3 RL (10), 5–12 RL (16)	5.1 ± 1 RL, 3.1 ± 0.2 SH, 3 ± 1 RL (10)	4* RL (1), 3–8* RL (2), ∼5.6* RL (9)	–
Baghan Quchan Bajgirab	4.7 ± 0.8 RL, 1.2 ± 0.7 SH	5.4 ± 1 RL, 2.1 ± 1 SH	2.8 ± 1 RL (8), 1* (4) 4.3 ± 0.6 RL (8), 1.5* (4) 1.5 RL * (4)	280 ± 16 (8) 83 ± 4 (8) –
Eastern Kopeh Dagh Binalud	2.4 ± 0.5 SH	2.7 ± 1 RL, 3.3 ± 1 SH	– 2.4 ± 0.5 (15) RL, 2.8 ± 0.6 (15) SH	– 2.8 ± 0.6 (15)
Koh Sorkh & Nishabur (59°E)	1.4 ± 0.7 SH		0.4-1.7 SH (11)	24.1 ± 1.9 (11)
Siah Koh & Sabzevar	1.0 ± 0.5 SH		<1 SH (3), 0.4–0.6 SH (11)	9–13 (3), 11 ± 2 (11)
Doruneh		2–3.5 LL, 1.5–2.8 SH	2.4 ± 0.3 (3)	10 (3)

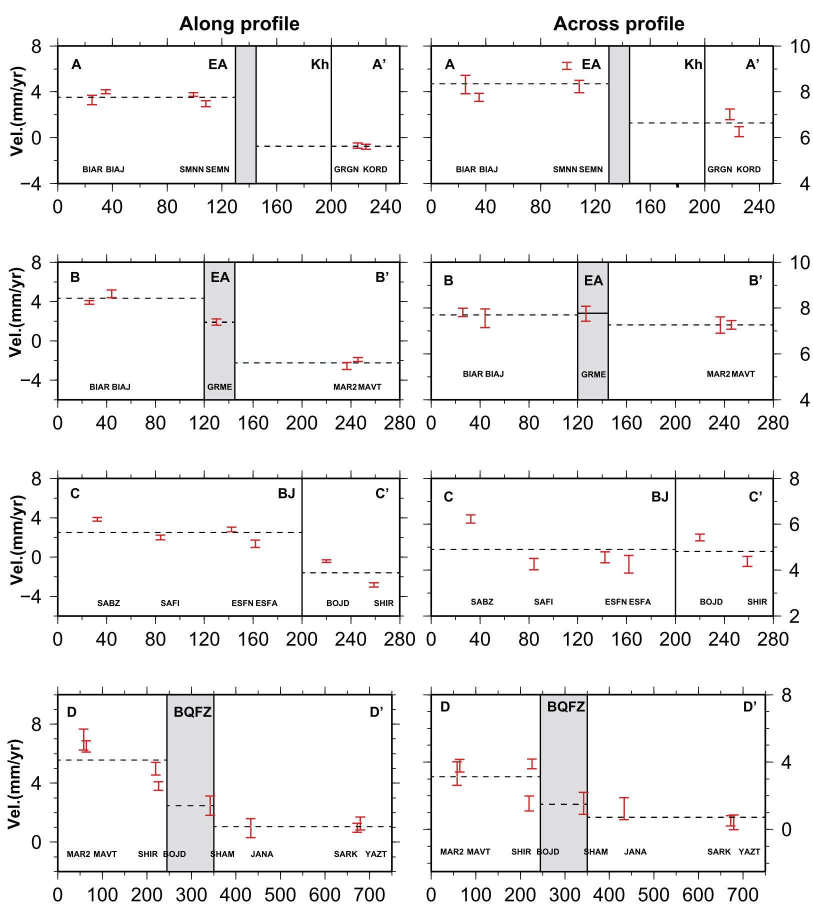

Fig. 5. Along (left) and across (right) velocity components (mm/yr) along profiles AA', BB', CC', and DD'. (See Fig. 2 for location of profiles.) Major active faults are marked as black lines and regions of known distributed faulting are highlighted in grey. Faults are labeled as in Fig. 1. East Alborz is Astaneh–Shahroud fault which is the major fault in the eastern Alborz. BQFZ is Barkharden–Quchan Fault Zone.

of 2.5 ± 1.0 mm/yr of left-lateral motion across Shahroud fault zone and 3.3 ± 1.0 mm/yr of left-lateral slip across Khazar thrust between longitude of 53°E to 56°E. There is no significant shortening across the zone (Fig. 4).

Further east, left-lateral strike-slip and shortening is accommodated across the Jajarm, Cheshmeh-Nik and Meyamay faults and Khazar thrust (Figs. 1 and 2). Fault-parallel velocities projected onto profile BB' (Fig. 5) show that the summed left-lateral strike-slip rate in this region is 6.5 ± 0.3 mm/yr. There is no significant shortening component across this part of the eastern Alborz (Figs. 2 and 5). Discriminating the individual slip-rates of the Meyamay, Jajarm and Cheshmeh-Nik faults is difficult, due to their close spacing. Station GRME is located very close to the Jajarm fault, and therefore, depending on the locking depth, it may be inside the deformation zone of this fault. If it is locked to a depth of less than 10 km, the GRME station can be located outside of the deformation zone. Then this station can be used to resolve the shear on individual faults. This would yield 4.1 ± 0.9 mm/yr of left-lateral movement for the Jajarm and Cheshmeh-Nik faults and 2.5 ± 0.9 mm/yr for the eastern part of Meyamay fault. However, the estimate of slip-rate for the Jajarm and Cheshmeh-Nik faults may be underestimated, and that of the Meyamay fault overestimated, respectively. Our block model yields 2.5 ± 1.0 mm/yr of left-lateral slip and 1.0 ± 1.0 mm/yr of shortening for the Cheshmeh-Nik–Jajarm system and for the Abr–Khaj fault system in its prolongation to the west.

At the eastern end of the Shahroud fault system, profile CC' shows 3.9 ± 1.4 mm/yr of left-lateral and 0.7 ± 1.0 mm/yr of shortening in the vicinity of Bojnord (Figs. 2 and 5). NE–SW left-lateral faults are visible in the geomorphology and geology in the vicinity of Bojnord but no late Quaternary slip-rate estimates exist on these structures (Hollingsworth et al. 2008, 2010b; Shabanian et al., 2009a, 2009b).

3.2. Western Kopeh Dagh and the Ashkabad fault

The South Caspian basin, which is an apparently rigid block of possible oceanic origin, is moving relative to both Eurasia and to central Iran (e.g. Jackson et al., 2002; Masson et al., 2007; Tavakoli, 2007; Djamour et al., 2010). Relative motion between the eastern part of the Caspian basin (in the eastern Caspian lowlands) and stable Eurasia to the north appears to be predominantly accommodated across the Ashkabad fault zone, which is the only major structure within this part of the collision zone, and which runs from the northern part of the eastern South Caspian basin to the central Kopeh Dagh (Fig. 1). The Ashkabad fault is located on the northern side of the eastern South Caspian basin and northwest of the Kopeh Dagh. The fault is a NW–SE right-lateral strike-slip fault with a thrust component and may have produced a large destructive earthquake ($M = 7.2$) in 1948 at Ashkabad (Trifonov, 1978; Priestley et al., 1994; Allen et al., 2004; Hollingsworth et al., 2008).

The variation of GPS velocities along profile DD' (Figs. 2 and 5) from SARK station on the Turan shield to MAVT/MAR2 stations in the Kopeh Dagh west of the Quchan fault zone (Fig. 2) indicates ~7 mm/yr of range-parallel extension along the trend of the Kopeh Dagh and Ashkabad fault. If the South Caspian motion relative to Eurasia can be represented by a rigid-body rotation about a pole sited far away (as we describe near the beginning of Section 3), this extension will represent the westward extrusion of the South Caspian Basin with respect to Eurasia. As we have no GPS measurements from the other side of the border in Turkmenistan we assume that the northern side of the Ashkabad fault has zero velocity with respect to Eurasia (as implied by the near zero velocity of YAZT further east, and by the lack of seismicity within the Turan platform). The variation of GPS velocities along profile DD' indicates 6.7 ± 0.5 mm/yr of right-lateral slip parallel to the Ashkabad fault and 3.4 ± 1.0 mm/yr of shortening perpendicular to it at longitude of ~56° (MAR2 and MAVT stations). These values decrease eastwards along the range, with 4.3 ± 0.5 mm/yr of right-lateral movement at station SHIR (consistent with the 3 ± 1 mm/yr estimated for the Ashkabad fault by Masson et al. (2007) using the SHIR station alone). There is also 2.6 ± 1.0 mm/yr of shortening at longitude 57°E (SHIR station). The component of velocity parallel to the Ashkabad fault decreases rapidly towards its eastern end with only ~2.4 mm/yr of right-lateral slip at the longitude of station SHAM. Our block model yields 5.1 ± 1.0 mm/yr of right-lateral slip and 3.1 ± 1.0 mm/yr of shortening across the Ashkabad fault zone. These values are higher than those calculated in the block model of Djamour et al. (2010). The differences arise both from the inclusion of more stations to define the south Caspian block and more measurement epochs to refine some of the older stations. However, the block model estimates are again substantially lower than those estimated from the profiles, which neglect any influence of rigid-body rotation of the South Caspian relative to Eurasia.

Support for a relatively fast slip-rate on the Ashkabad fault comes from an estimate of 5–12 mm/yr, with a best-fit at 9 mm/yr, obtained from the accumulation of interseismic strain imaged with InSAR (Walters et al., 2013). The interseismic strain-rate measured across the Ashkabad fault thus agrees with our GPS-derived estimate of 6.7 ± 0.5 mm/yr for the right-lateral slip-rate on the central Ashkabad fault and provides additional support that the motion of the South Caspian Basin may approximate as a rotation about a far-away Euler pole, corresponding to a motion at a rate and direction represented by stations MAR2 and MAVT.

3.3. Central Kopeh Dagh and the Barkharden–Quchan Fault Zone

The central Kopeh Dagh is cut by a series of four major NNW-SSE right-lateral strike-slip faults of the Barkharden–Quchan Fault Zone (BQFZ) that are named, from west to east, the Shirvan, Baghan, Quchan and Dorvadam faults (Hollingsworth et al., 2006; Shabanian et al., 2009a) (Fig. 1). Hollingsworth et al. (2006) proposed that the faults accommodate N–S convergence by a combination of right-lateral faulting and anticlockwise block rotation about a vertical axis, whereas Shabanian et al. (2009b) suggest instead that Central Iran and the Kopeh Dagh are translated northwestward with respect to Eurasia by localized strike-slip faulting through the BQFZ.

Approximately 4.5 ± 1.2 mm/yr of N–S shortening is accommodated across the central Kopeh Dagh (the northward velocity of stations ESFA/ESFN with respect to Eurasia) (Fig. 2). However, our GPS stations are too sparse to estimate the slip-rate of the individual faults within the BQFZ, and we instead estimate the overall motions across the zone. Fault-parallel and fault-normal velocities calculated from the block modeling for the BQFZ indicate 5.2 ± 1.0 mm/yr of right-lateral displacement and 2.1 ± 1.0 mm/yr of shortening summed across the zone (Figs. 4 and 5). Masson et al. (2007) used the difference in velocity between stations SHIR and MSHN to estimate a slip-rate for the BQFZ. They obtained 3 ± 1 mm/yr of elongation along-strike of the Kopeh Dagh at the longitude of SHIR station (57°E).

3.4. The eastern Kopeh Dagh, Binalud and Koh-e-Sorkh ranges

Northward-directed GPS velocities relative to Eurasia show that contraction across NE Iran is accommodated in the eastern Kopeh Dagh and, further to the south, across the Binalud, Siah Koh and Koh-e-Sorkh ranges (Fig. 1; Hollingsworth et al., 2006). It is probable that additional shortening is accommodated on faults south of Koh-e-Sorkh and on additional structures within NE Iran (e.g.

Hollingsworth et al., 2010a). The amount of shortening varies with longitude, with the northward velocity with respect to Eurasia decreasing eastwards, reaching zero near the Afghan border. At longitude ∼59°E we estimate a total of 4.5 ± 0.5 mm/yr of N–S shortening between stations KSHM (or THED) and YAZT. Our estimate refines the previous rate of 5.0 ± 0.9 mm/yr by Masson et al. (2007). The wide distribution of active faulting and seismicity within the region is visible in Fig. 1.

A number of permanent and campaign stations were installed in this eastern part of our area in order to provide details of strain accumulation in the vicinity of the large cities of Mashhad and Nishabur. However, the GPS data in this part of our network are affected by high rates of subsidence caused by water extraction. For instance, using GPS, InSAR and leveling data, Motagh et al. (2007) measured 15 cm/yr of subsidence in the Mashhad Valley during the period 2003–2005. Our GPS vertical velocity estimations can give the gross value of subsidence for this area. We obtain 214, 89, 51, 9 and 3 mm/yr of subsidence for stations TOUS, NISH, NFRD, GOLM and KALT, respectively. Although some of these stations yield horizontal velocities that are consistent in magnitude and azimuth with surrounding stations, the horizontal movements can potentially be influenced by the subsidence of the area and therefore we do not use them in our analysis.

According to block modeling, there is 2.4–3.5 mm/yr of right-lateral slip and 2.7–3.3 mm/yr of shortening across the Binalud and Kopeh Dagh region (Fig. 4). The difference between the velocities of ZVNG and SARK/YAZT, located respectively to the south and north of the ranges, indicates 2.4 ± 0.5 of shortening across the Binalud and the eastern part of Kopeh Dagh at a longitude of ∼59°E. The distribution of the GPS velocities (Fig. 2) suggests that most of this deformation may accumulate in the Binalud rather than within the Kopeh Dagh region. The strike-slip and shortening deformation in this area may be partitioned on right-lateral and thrust faults. The strike-slip component might be accommodated on one single fault (the Nishabur fault, for instance), which is consistent with the model proposed by Shabanian et al. (2009b), or on right-lateral faults within the Binalud mountains (Hollingsworth et al., 2010a). Hollingsworth et al. (2010a) determined the late Quaternary rate of shortening across the Nishabur fault to be 0.4–1.7 mm/yr by OSL dating of vertically displaced alluvial terraces. Shabanian et al. (2012) provide a larger estimate of 2.4 ± 0.5 and 2.8 ± 0.6 mm/yr for right-lateral and reverse components of slip (corresponding to an oblique slip-rate of 3.6 ± 1.0 mm/yr) across the Nishabur fault using in *situ*-produced ^{10}Be exposure dating. The rates calculated by Shabanian et al. (2012) suggest that most of the shortening between ZVNG and SARK/YAZT is accommodated across the Nishabur fault, whereas the lower estimate by Hollingsworth et al. (2010a) indicates that other structures in the region may still be important. Earthquakes within the region east of longitude ∼57°E mostly have reverse faulting mechanisms (Fig. 1). The earthquake slip-vector azimuths are directed N to NNE, orthogonal to the local strike of the range-bounding reverse faults, and suggesting that right-lateral strike-slip faulting occurs within these ranges as a consequence of oblique slip (Hollingsworth et al., 2008).

The 1.0 ± 0.6 mm/yr difference in velocity between stations GONA and KSHM is likely accommodated on reverse faults between Kashmar and Gonabad. Further west, the difference between DARG and SAFI stations indicates possible activity of 1.0 ± 0.5 mm/yr of shortening across the Siah Koh mountain belt and the Sabzevar reverse fault (Fig. 2). The SABZ station is located exactly on the Sabzevar thrust, so it is not possible to separate the contributions to the deformation from the Sabzevar fault and other potential faults within the Siah Koh mountain range. Fattahi et al. (2006a) estimate a Holocene shortening rate of 0.4–0.6 mm/yr across the Sabzevar fault. However, a rate of ∼1 mm/yr is possible if the reverse fault flattens into a decollement at depth (Hollingsworth et al., 2010a).

South of latitude 36°N the major structures are the E–W Doruneh and Dasht-e-Bayaz left-lateral faults. Fattahi et al. (2006b) estimate ∼2.5 mm/yr for the Holocene left-lateral slip-rate across the Doruneh fault. Our block model yields ∼2 mm/yr of left-lateral slip along the eastern part of the Doruneh fault, rising to 3.5 mm/yr in the west.

4. Discussion

Our geodetic measurements add new constraints on the rates of faulting and the present-day kinematics of major fault zones in NE Iran. In North East Iran, a striking feature of the velocity field is that the vectors across the entire eastern and southern parts of the network are directed northwards relative to Eurasia (Fig. 2). The northward-directed velocities decrease linearly towards the eastern border of Iran, they also decrease smoothly towards the northern border. This distribution of velocities suggests a broad zone of N–S right-lateral shearing through eastern Iran that must be accompanied by clockwise rotation about a vertical axis, which is seen in the kinematic block model (Fig. 4). An important consequence of the observed GPS velocities is that the shear is not localized in a narrow zone at the eastern border of Iran as envisaged by Shabanian et al. (2009b).

Further west, there is an abrupt change in the orientation in the velocity vectors across the Shahroud fault zone in the eastern Alborz, such that all vectors north and west of the eastern Alborz point northwest relative to Eurasia. These velocities have been used to describe the motion of the South Caspian basin as a clockwise rigid-body rotation about an Euler pole sited near the eastern Kopeh Dagh (Djamour et al., 2010). However, most of the existing GPS measurements used to constrain the motion of the South Caspian are sited close to its margins, as the interior of the basin is mostly covered by water. Two stations (MAVT and MAR2) that we have presented for the first time in this paper have velocities that are not consistent with the rigid-body rotation about a near-by rotation pole as defined by the remainder of the Caspian stations. The velocities of MAVT and MAR2 are, however, consistent with the motions predicted from plate-closure models (Jackson et al., 2002; Copley and Jackson, 2006). Although we cannot rule out significant rotation of the South Caspian about a near-by pole, our new GPS data, along with an independent constraint on fast interseismic strain accumulation across the Ashkabad fault (Walters et al., 2013), indicate that its motion is likely to be a clockwise rotation relative to Eurasia about a pole that is much further away than that calculated by Djamour et al. (2010).

A consequence of the resulting northwest motion of the South Caspian region relative to Eurasia is that it must introduce extension between the eastern Caspian lowlands and the eastern Kopeh Dagh (which is moving northwards relative to Eurasia). The difference in the velocities of stations JANA and SHIR projected onto a profile parallel to the trend of the Kopeh Dagh show that ∼7 mm/yr of extension is accommodated in a narrow zone of the central Kopeh Dagh (Figs. 2, 5). This range-parallel extension, which has a trend of ∼N35°W, is coincident with the right-lateral strike-slip faults of the BQFZ. Hollingsworth et al. (2006) provide a scenario of 'bookshelf faulting' that can account for the observed deformation across the BQFZ. An important consequence of the bookshelf model of faulting is that the slip-rates across individual faults within the BQFZ cannot simply be summed to find the overall rates of deformation across the zone. Instead, the slip-rates on the faults are related to the along-strike extension and across-strike shortening and vary depending on the width of the fault-bounded blocks and the rates of vertical axis rotation. We estimate 3.3-5.4 mm/yr of cumulative right-lateral slip across the BQFZ in the central Kopeh Dagh. The summed right-lateral bedrock displacement across the zone is ∼45 km (Hollingsworth et al., 2006; Shabanian et al., 2009a). At the present-day rate, the 45 km of displacement would accumulate in 8.3–15 Ma. Shabanian et al. (2009a) estimate long-term slip-rates of 2.8 ± 1.0 mm/yr and 4.3 ± 0.6 mm/yr for the Baghan and Quchan faults, respectively, which, given that they displace bedrock right-laterally by 10 km and 15 km, may have started as little as 4 Ma ago. The cumulative GPS slip-rate across the BQFZ faults is consistent with the lower boundary of the sum of the long-term slip-rates on the Baghan and Quchan faults. These two faults appear to accommodate the major part of right-lateral displacement in the BQFZ, but this comparison does not take into account any anticlockwise vertical axis rotation that might occur in allowing the faults to accommodate extension between the eastern Kopeh Dagh and the South Caspian (e.g. Hollingsworth et al. 2006, 2008, 2010a).

Comparison of our geodetic slip-rates with geological rates allows us to test for agreement between slip-rates derived over different timescales. Comparison with long-term geological estimates of displacement across the faults also permits us to provide constraints on the possible timing of initiation of faulting. In Table 2 we summarize the geodetic short-term (decadal) slip-rate estimates derived from our GPS velocities and include the long-term (late Quaternary) estimates where available. Comparison of these two sets show that the two estimates generally agrees, indicating that the GPS velocities can be reasonably extrapolated to be representative of fault slip-rates over the last ∼10 ka. If this is the case, for faults with only GPS-based slip estimates, our geodetic results allow us to infer long-term slip-rates for the left-lateral faults of eastern Alborz east of 55°E.

In the eastern Alborz, the strike-slip component and shortening are accommodated on the Astaneh segment of the Shahroud fault system and the Khazar thrust (Figs. 2, 4 and 5). At a longitude of 55°E, the GPS velocity field (both in the AA' and BB' profiles and in the block modeling) shows 4.4–6.5 mm/yr of left-lateral displacement and 0.5–2 mm/yr of shortening across the eastern part of the Shahroud fault and Khazar thrust. This amount agrees with existing late Quaternary slip-rate estimates of 3–4 mm/yr and 1–3 mm/yr of right-lateral slip across the Abr and Khij Faults (Javidfakhr et al., 2011a), which are the two main active strands at the longitude of Profile AA', and which do not show any obvious component of dip-slip in the geomorphology. Comparison between geologic and geodetic slip-rates hence suggests that most of the strike-slip component occurs south of Alborz range, while the shortening component is accommodated north of the range (Djamour et al., 2010).

Djamour et al. (2010) used GPS measurements to evaluate 2 ± 1 mm/yr of left-lateral displacement rate for the Astaneh fault, at the far western end of our study region. Hollingsworth et al. (2010b) suggested 1.7–2.5 mm/yr of slip-rate for the Astaneh fault – the SW section of the left-lateral Shahroud fault system – by assuming the 50–60 m fan offset in this region has been accommodated in the last 22–30 kyr. Rizza et al. (2011) measured a maximum left-lateral slip-rate of 2.0 ± 0.3 mm/yr by IRSL dating of geomorphic features displaced 112 ± 15 m across the Astaneh fault at a longitude of 54°E. The 30–40 km total offset across the Astaneh section of Shahroud fault system proposed by Hollingsworth et al. (2008) would accumulate in 13–23.5 Ma at the late Quaternary rates of Rizza et al. (2011), or in 10–40 Ma if it accommodates all the left-lateral shearing observed by GPS (Djamour et al., 2010). Ritz (2009), however, suggests the total displacement across the Astaneh fault is much less than 30–40 km, such that the fault may have initiated later.

The Kopeh Dagh, the mountain range at the northern limit of the Arabian–Eurasian collision zone, accommodates the northernmost part of the NS convergence. Considering the GPS velocity field, the Kopeh Dagh can be divided in 3 parts; west, central and east. The western Kopeh Dagh is accommodating, together with the Shahroud fault system, the westward extrusion of the South Caspian basin. Here, the right-lateral Ashkabad fault shows close to ∼ 5 mm/yr of along-strike motion (if the South Caspian motion involves a clockwise rotation about a nearby pole, as seen in the block modeling results) and up to 6.7 ± 0.5 mm/yr at the longitude of Maraveh–Tapeh as estimated from the profile D–D′ (Fig. 5), with this figure reducing to 4.3 ± 0.5 mm/yr at the longitude of Shirvan. The westward motion therefore decreases towards the east. The geodetic rates are consistent with the 3–8 mm/yr geological estimation of Lyberis and Manby (1999). They are also consistent with InSAR-constrained interseismic strain accumulation across the Ashkabad fault at a rate of 5–12 mm/yr (Walters et al., 2013). Our estimate is larger than the ∼ 4 mm/yr estimated from the displacement of a Qanat (an underground water canal) suggesting that it is younger than the ∼2.5 ka age assumed by Trifonov (1978). A total geological right-lateral offset of 35 km was recognized close to SHIR station (Lyberis and Manby, 1999; Hollingsworth et al., 2008), though we note that the robustness of the geological displacements has been the matter of some discussion (Ritz, 2009; Siame et al., 2009; Hollingsworth et al., 2009). If we assume that the presently measured geodetic slip-rate of ∼5 mm/yr on the Ashkabad fault at SHIR station has been constant throughout its history, the initiation of strike-slip faulting would have been at ∼7 Ma. If, however, the 35 km of displacement accumulated at the full rate of 6.7 ± 0.5 mm/yr measured further west on the Ashkabad fault, the faulting may be as young as ∼5 Ma.

The eastern part of the Kopeh Dagh, according to the GPS velocity field (Fig. 2), absorbs NS shortening between SARK and MSHN. If we consider that most of the 3.2 ± 1.5 mm/yr of shortening between ZVNG and Eurasia is accommodating in the Binalud, assuming a constant shortening rate since initiation of faulting, it takes 20–24 Ma to accommodate the ∼60 km shortening across Binalud which is proposed by Hollingsworth et al. (2006). If we assume that the ∼30 km of total NS shortening across the eastern Alborz can apply for Binalud, it takes 12 Ma to accommodate this shortening across Binalud.

5. Conclusion

A regional deformation field has been estimated from GPS measurements that covers NE Iran and shows that distributed right-lateral shearing is accommodated across a wide part of eastern Iran. In the NE, this right-lateral shearing is converted into shortening across the Koh-e-Sorkh, Binalud and Kopeh Dagh ranges. At the longitude of Kashmar, the N–S shortening is at a rate of $\sim 4.5 \pm 0.5$ mm/yr, which decreases toward the east and dies out at the Afghanistan border. Our new GPS data suggest that the South Caspian Basin is moving at up to ∼7 mm/yr relative to Eurasia at an azimuth of 317°N, constraining a rigid block rotation around an Euler pole that is further away than previously thought. This maximum relative motion between the South Caspian Basin and its surroundings would result in ∼7 mm/yr of right-lateral strike-slip motion along the Ashkabad Fault and 4 to 6.5 mm/yr of left-lateral strike-slip motion within the eastern Alborz Mountains (profile BB') depending on the locking depth of the fault system. These estimates are much faster than previously assumed, though there is additional support for a fast slip-rate on the Ashkabad fault from measurements of elastic strain accumulation (Walters et al., 2013), and highlight a potentially acute hazard associated with these fault zones, particularly given the overall lack of recent or historic earthquakes on them. Testing our assertions requires further GPS stations in the eastern Caspian lowlands to determine the South Caspian motion, and direct measurements of the slip-rate of the main faults of the eastern Alborz.

Acknowledgements

We would like to thank the National Cartographic Center in Tehran for the Iranian Permanent GPS Network (IPGN), in particular NCC head Mr Ilkhan and Mr Vazei. We are grateful to the Geodynamic Department in Iran, special thanks to Z. Rahimi, S. Hosseini, F. Khorrami, M. Alijanzadeh and N. Eftekharzadeh. The campaign measurements have been supported by the French CNRS-INSU, the National Cartographic Center (NCC Tehran) and the International Institute of Earthquake Engineering and Seismology (IIEES-Tehran). We thank all the people who did the field work to collect the data, in particular Mr Hendi, Mr Rahmani, Mr Sardari and Mr Nemati. We acknowledge the support of OSUG (Observatoire des Sciences de l'Univers de Grenoble) for a Visiting Fellowship awarded to RTW. F. Nilforoushan is funded by the Swedish research council (VR). We value detailed and informative comments on an earlier version of the paper by P. Vernant and M. Floyd.

References

Allen, M.B., Ghassemi, M.R., Shahrabi, M., Qorashi, M., 2003. Accommodation of late Cenozoic oblique shortening in the Alborz range, northern Iran. J. Struct. Geol. 25, 659–672.

Allen, M., Jackson, J., Walker, R., 2004. Late Cenozoic reorganization of the Arabia–Eurasia collision and the comparison of short-term and long-term deformation rates. Tectonics 23, TC2008, http://dx.doi.org/10.1029/2003TC001530.

Altamimi, Z., Collilieux, X., Métivier, L., 2011. ITRF2008: an improved solution of the International Terrestrial Reference Frame. J. Geod. 85 (8), 457–473.

Ambraseys, N., Melville, C., 1982. A History of Persian Earthquakes. Cambridge University Press, Cambridge.

Baker, C., Jackson, J., Priestley, K., 1993. Earthquakes on the Kazerun Line in the Zagros Mountains of Iran: strike-slip faulting within a fold-and-thrust belt. Geophys. J. Int. 115 (1), 41–61.

Berberian, M., Yeats, R.S., 1999. Patterns of historical earthquake rupture in the Iranian Plateau. Bull. Seismol. Soc. Am. 89, 120–139.

Boehm, J., Werl, B., Schuh, H., 2006. Troposphere mapping functions for GPS and very long baseline interferometry from European Centre for Medium-Range Weather Forecasts operational analysis data. J. Geophys. Res. 111, B02406, http://dx.doi.org/10.1029/2005JB003629.

Copley, A., Jackson, J., 2006. Active tectonics of the Turkish–Iranian Plateau. Tectonics 25, TC6006, http://dx.doi.org/10.1029/2005TC001906.

Djamour, Y., Vernant, P., Bayer, R., Nankali, H.R., Ritz, J.F., Hinderer, J., Hatam, Y., Luck, B., LeMoigne, N., Sedighi, M., Khorrami, F., 2010. GPS and gravity constraints on continental deformation in the Alborz mountain range, Iran. Geophys. J. Int. 183, 1287–1301.

Djamour, Y., Vernant, P., Nankali, H.R., Tavakoli, F., 2011. NW Iran–eastern Turkey present-day kinematics: Results from the Iranian permanent GPS network. Earth Planet. Sci. Lett. 307 (1), 27–34.

Engdahl, E., Jackson, J., Myers, S., Bergman, E., Priestley, K., 2006. Relocation and assessment of seismicity in the Iran region. Geophys. J. Int. 167, 761–788.

Fattahi, M., Walker, R., 2007. Luminescence dating of the last earthquake of the Sabzevar thrust fault, NE Iran. Quart. Geochronol. 2, 284–289.

Fattahi, M., Walker, R., Hollingsworth, J., Bahroudi, A., Nazari, H., Talebian, M., Armitage, S., Stokes, S., 2006a. Holocene slip-rate on the Sabzevar thrust fault, NE Iran, determined using optically stimulated luminescence (OSL). Earth Planet. Sci. Lett. 245 (3–4), 673–684.

Fattahi, M., Walker, R., Khatib, M., Dolati, A., Bahroudi, A., 2006b. Slip-rate estimate and past earthquakes on the Doruneh fault, eastern Iran. Geophys. J. Int. 168 (2), 691–709.

Gelb, A., 1974. Applied Optimal Estimation. MIT Press, Cambridge, MA.

Herring, T.A., King, R.W., McClusky, S.C., 2006. Introduction to GAMIT/GLOBK, Release 10.3. Dept. of Earth Atmos. and Planet. Sci., Mass. Inst. of Technol., Cambridge, MA.

Hessami, K., Nilforoushan, F., Talbot, C., 2006. Active deformation within the Zagros Mountains deduced from GPS measurements. J. Geol. Soc. 163, 143–148.

Hollingsworth, J., Jackson, J., Walker, R., Gheitanchi, M., Bolourchi, M., 2006. Strike-slip faulting, rotation, and along-strike elongation in the Kopeh Dagh mountains, NE Iran. Geophys. J. Int. 166, 1161–1177.

Hollingsworth, J., Jackson, J., Walker, R., Nazari, H., 2008. Extrusion tectonics and subduction in the eastern South Caspian region since 10 Ma. Geology 36 (10), 763–766.

Hollingsworth, J., Jackson, J., Walker, R., Nazari, H., 2009. Extrusion tectonics and subduction in the eastern South Caspian region since 10 Ma: reply. Geology 37 (12), 199–200.

Hollingsworth, J., Fattahi, M., Walker, R., Talebian, M., Bahroudi, A., Bolourchi, M., Jackson, J., Copley, A., 2010a. Oroclinal bending, distributed thrust and strike-slip faulting, and the accommodation of Arabia–Eurasia convergence in NE Iran since the Oligocene. Geophys. J. Int. 181, 1214–1246.

Hollingsworth, J., Nazari, H., Ritz, J.-F., Salamati, R., Talebian, M., Bahroudi, A., Walker, R., Rizza, M., Jackson, J., 2010b. Active tectonics of the east Alborz mountains, NE Iran: rupture of the left-lateral Astaneh fault system during the great 856 A.D. Qumis earthquake. J. Geophys. Res. 115, B12313.

Jackson, J., Priestley, K., Allen, M., Berberian, M., 2002. Active tectonics of the South Caspian Basin. Geophys. J. Int. 148, 214–245.

Javidfakhr, B., Bellier, O., Shabanian, E., Siame, L., Léanni, L., Bourlès, D., Ahmadian, S., 2011a. Fault kinematics and active tectonics at the southeastern boundary of the eastern Alborz (Abr and Khij fault zones): geodynamic implications for NNE Iran. J. Geodyn. 52, 290–303.

Javidfakhr, B., Bellier, O., Shabanian, E., Ahmadian, S., Saidi, A., 2011b. Plio–Quaternary tectonic regime changes in the transition zone between Alborz and Kopeh Dagh mountain ranges (NE Iran). Tectonophysics 506, 86–108.

Karakhanyan, A., Vernant, P., Doerflinger, E., Avagyan, A., Philip, H., Aslanyan, R., Champollion, C., Arakelyan, S., Collard, P., Baghdasaryan, H., Peyret, M., Davtyan, V., Calais, E., Masson, F., 2013. GPS constraints on continental deformation in the Armenian region and Lesser Caucasus. Tectonophysics 592, 39–45.

Lyard, F., Lefèvre, F., Letellier, T., Francis, O., 2006. Modeling the global ocean tides: A modern insight from FES2004. Ocean Dyn. 56, 394–415.

Lyberis, N., Manby, G., 1999. Oblique to orthogonal convergence across the Turan block in the post-Miocene. Am. Assoc. Pet. Geol. Bull. 83 (7), 1135–1160.

Mangino, S., Priestley, K., 1998. The crustal structure of the southern Caspian region. Geophys. J. Int. 133, 630–648.

Masson, F., Chery, J., Hatzfeld, D., Martinod, J., Vernant, P., Tavakoli, F., Ghafory-Ashtiani, M., 2005. Seismic versus aseismic deformation in Iran inferred from earthquakes and geodetic data. Geophys. J. Int. 160 (1), 217–226.

Masson, F., Anvari, M., Djamour, Y., Walpersdorf, A., Tavakoli, F., Daignières, M., Nankali, H., Van Gorp, S., 2007. Large-scale velocity field and strain tensor in Iran inferred from GPS measurements: new insight for the present-day deformation pattern within NE Iran. Geophys. J. Int. 170, 436–440.

McCaffrey, R., 2002. Crustal block rotations and plate coupling. In: Stein, S., Frey Mueller, J.T. (Eds.), Plate Boundary Zones. In: AGU Geodyn. Ser., pp. 101–122.

McKenzie, D., 1972. Active tectonics of the Mediterranean region. Geophys. J. R. Astron. Soc. 30 (2), 109–185.

Meade, B.J., Hager, B.H., 2005. Block models of crustal motion in southern California constrained by GPS measurements. J. Geophys. Res. 110, B04402.

Meade, B.J., Hager, B.H., McClusky, S., Reilinger, R., Ergintav, S., Lenk, O., Barka, A., Özener, H., 2002. Estimates of seismic potential in the Marmara Sea regions from block models of secular deformation constrained by Global Positioning System Measurements. Bull. Seismol. Soc. Am. 92, 208–215.

Meyer, B., Le Dortz, K., 2007. Strike-slip kinematics in Central and Eastern Iran: estimating fault slip-rates averaged over the Holocene. Tectonics 26, TC5009.

Motagh, M., Djamour, Y., Walter, T.R., Wetzel, H.-U., Zschau, J., Arabi, S., 2007. Land subsidence in Mashhad Valley, northeast Iran: results from InSAR, levelling and GPS. Geophys. J. Int. 168 (2), 518–526.

Nilforoushan, F., et al., 2003. GPS network monitors the Arabia–Eurasia collision deformation in Iran. J. Geod. 77, 411–422.

Okada, Y., 1985. Surface deformation due to shear and tensile faults in a half-space. Bull. Seismol. Soc. Am. 75, 1135–1154.

Priestley, K., Baker, C., Jackson, J., 1994. Implications of earthquake focal mechanism data for the active tectonics of the south Caspian basin and surrounding regions. Geophys. J. Int. 118, 111–141.

Reilinger, R., et al., 2006. GPS constraints on continental deformation in the Africa–Arabia–Eurasia continental collision zone and implications for the dynamics of plate interactions. J. Geophys. Res. 111, B05411.

Ritz, J.-F., 2009. Extrusion tectonics and subduction in the eastern South Caspian region since 10 Ma: Comment. Geology 37, e191.

Rizza, M., Mahan, S., Ritz, J.-F., Nazari, H., Hollingsworth, J., Salamati, R., 2011. Using luminescence dating of coarse matrix material to estimate the slip rate of the Astaneh fault, Iran. Quart. Geochronol. 6 (3–4), 390–406.

Shabanian, E., Siame, L., Bellier, O., Benedetti, L., Abbassi, M.R., 2009a. Quaternary slip rates along the northeastern boundary of the Arabia–Eurasia collision zone (Kopeh Dagh Mountains, Northeast Iran). Geophys. J. Int. 178, 1055–1077.

Shabanian, E., Bellier, O., Siame, L., Arnaud, N., Abbassi, M.R., Cochemé, J.-J., 2009b. New tectonic configuration in NE Iran: Active strike-slip faulting between the Kopeh Dagh and Binalud mountains. Tectonics 28, TC5002, http://dx.doi.org/10.1029/2008TC002444.

Shabanian, E., Bellier, O., Siame, L., Abbassi, M.R., Bourlès, D., Braucher, R., Farbod, Y., 2012. The Binalud Mountains: A key piece for the geodynamic puzzle of NE Iran.

Siame, L.L., Shabanian, E., Bellier, O., 2009. Extrusion tectonics and subduction in the eastern South Caspian region since 10 Ma: Comment. Geology 37 (12), 197–198.

Talebian, M., Jackson, J., 2004. A reappraisal of earthquake focal mechanisms and active shortening in the Zagros mountains of Iran. Geophys. J. Int. 156 (3), 506–526.

Tatar, M., Hatzfeld, D., Martinod, J., Walpersdorf, A., Ghafori-Ashtiany, M., Chéry, J., 2002. The present-day deformation of the central Zagros from GPS measurements. Geophys. Res. Lett. 29 (19).

Tatar, M., Jackson, J., Hatzfeld, D., Bergman, E., 2007. The 2004 May 28 Baladeh earthquake (Mw 6.2) in the Alborz, Iran: overthrusting the South Caspian Basin margin, partitioning of oblique convergence and the seismic hazard of Tehran. Geophys. J. Int. 170, 249–261.

Tavakoli, F., 2007. Present-day kinematics of the Zagros and east of Iran faults. PhD thesis. Univ. of Joseph Fourier, Grenoble, France.

Tavakoli, F., Walpersdorf, A., Authemayou, C., Nankali, H.R., Hatzfeld, D., Tatar, M., Djamour, Y., Nilforoushan, F., Cotte, N., 2008. Distribution of the right-lateral strike-slip motion from the Main Recent Fault to the Kazerun Fault System (Zagros, Iran): Evidence from present-day GPS velocities. Earth Planet. Sci. Lett. 275 (3–4), 342–347, http://dx.doi.org/10.1016/j.epsl.2008.08.030.

Trifonov, V., 1978. Late quaternary tectonic movements of western and central Asia. Geol. Soc. Am. Bull. 89, 1059–1072.

Vernant, P., et al., 2004. Present-day crustal deformation and plate kinematics in the Middle East constrained by GPS measurements in Iran and northern Oman. Geophys. J. Int. 157 (1), 381–398.

Walker, R., Jackson, J., 2004. Active tectonics and late Cenozoic strain distribution in central and eastern Iran. Tectonics 23, TC5010.

Walpersdorf, A., et al., 2006. Difference in the GPS deformation pattern of north and central Zagros (Iran). Geophys. J. Int. 167 (3), 1077–1088.

Walters, R.J., Elliott, J.R., Li, Z., Parsons, B., 2013. Rapid strain accumulation on the Ashkabad fault (Turkmenistan) from atmosphere-corrected InSAR. J. Geophys. Res., http://dx.doi.org/10.1002/jgrb.50236.